Journal of Inorganic and Organometallic Polymers and Materials
https://doi.org/10.1007/s10904-021-02186-9

Green Biogenic Synthesis of Silver Nanoparticles Using Aqueous Extract of *Moringa Oleifera:* Access to a Powerful Antimicrobial, Anticancer, Pesticidal and Catalytic Agents

Laila H. Abdel-Rahman[1] · Badriah Saad Al-Farhan[2] · Doaa Abou El-ezz[3] · M. A. Abd–El Sayed[4] · Mallak Megalea Zikry[4] · Ahmed M. Abu-Dief[1,5]

Received: 18 October 2021 / Accepted: 6 December 2021

Abstract
In this study, we look into the biogenic synthesis of (AgNPs) utilizing a simple and environmentally friendly method based on an aqueous extract of *Moringa Oleifera* (MO). The synthesized MOAgNPs were characterized using a UV–Visible spectrophotometry, X-ray diffraction (XRD), Fourier transform infrared (FT-IR) spectra and TEM image which confirmed the spherical shape of MOAgNPs with particle size range of 5–50 nm with an average particle size of 38.7 nm. Significantly, the prepared MOAgNPs showed high pesticidal activity towards *Spodoptera littoralis*. MOAgNPs also exhibited strong antibacterial activities against Gram-positive and Gram-negative bacteria. The prepared MOAgNPs were screened for their cytotoxic effect against (HCT-116), (HepG-2) and (MCF-7) carcinoma cell lines. Finally, the synthesized MOAgNPs have been used as a catalyst for the reduction of 2,4-Dinitrophenol using $NaBH_4$ to 2,4-Diaminophenol. Taken together, the outstanding catalytic and biological activities of the synthesized MOAgNPs entitled them for applications as catalyst, pesticidal, antibacterial and anticancer agents in medical applications.

Keywords Green method · Silver nanoparticles · Pesticide · Anticancer · Antibacterial · *Spodoptera littoralis* · *Moringa oleifera* · Catalytic reduction

1 Introduction

Because of their properties in comparison to the bulk version of the same element, nanomaterials are extremely important. Nanomaterials have a variety of properties that are dependent on the shape and size of the nanoparticles [1–3]. The methods for chemically nanoparticle synthesis are dangerous and costly. Several researchers have produced silver nanoparticles (AgNPs) using chemical, biological, and environmentally friendly methods [4–6]. Because of the increased surface area, the green approach of nanoparticle manufacturing boosts catalytic activity [7]. Various plant extracts have been investigated for nanomaterial production, including copper and zinc [8], gold and magnesium [9], and silver [10, 11]. Silver shows low toxicity in humans [12]. AgNPs have a positive impact on infection treatment because they break bacterial cell walls, resulting in cell death [13]. Because of their cytotoxic effects on tumor cells, AgNPs play an important function in medicine. [14, 15]. Normal cells are not harmed by AgNPs made using environmentally friendly procedures [16]. AgNPs can be produced from a variety of plants [17]. As a reducing and capping agent, we utilized Moringa Oleifera extract for AgNPs biosynthesis. It can be found at the Shandaweel Research Center.

Moringa Oleifera is a potential substance for addressing nutritional insufficiency and metabolic imbalance in people [18]. Moringa is used as a traditional medicinal plant that

✉ Laila H. Abdel-Rahman
laila.abdelrahman@science.sohag.edu.eg;
lailakenawy@hotmail.com

1 Chemistry Department, Faculty of Science, Sohag University, Sohâg 82534, Egypt

2 Chemistry Department, Faculty of Girls for Science, King Khalid University, Abha, Saudi Arabia

3 Department of Pharmacology and Toxicology, Faculty of Pharmacy, October University for Modern Sciences and Arts (MSA University), Giza, Egypt

4 Medicinal and Aromatic Plants Researches Department, Horti. Res. Institute (H.R.I.), Agri. Res. Center (A.R.C.), Giza, Egypt

5 Department of Chemistry, College oaf Science, Taibah University, P.O. Box 344, Medina, Saudi Arabia

Published online: 24 January 2022

provides better nourishment due to the presence of certain critical nutrients in its leaves [19, 20]. Despite its potential as a future option for undernutrition therapy in clinical or biomedical settings, Moringa oleifera is required for the production of biomaterials or green materials in advanced bioengineering [21, 22]. *Moringa oleifera* is used for bone healing [23], ZnO nanomaterials synthesis with high electrochemical activity [24, 25], NiO nanoparticles synthesis with anticancer activity [26, 27], TiO_2 nanoparticles synthesis that is used for wound healing [28], antibacterial agent [29] and heavy metal ions (Pb^{2+} and Cd^{2+}) adsorption.

As a result of the biomaterials' simplicity, stability, and biocompatibility, leaf powder from local bioresources was chosen for analysis of chemical properties and prospective applications in this study. Despite some preliminary laboratory work on the green synthesis of moringa nanoparticles, there is little information on how the Madura variety resulted in the important chemical and structural features of moringa leaf powder. Furthermore, no information on the manufacturing of biomaterials from Madura moringa is available. The use of *Moringa oleifera* and other plants in the synthesis of silver nanoparticles is leading to truly green chemistry, which is more cost-effective and environmentally benign than chemical and physical methods and can be easily scaled up for large scale syntheses [30, 31].

Spodoptera littoralis (cotton leaf worm) is a species of moth in the Noctuid family that is harmed by AgNPs. Female moths can lay anything from 20 to 1000 eggs. *S. littoralis* larvae have been found to eat a variety of plant species and families. *S. littoralis* feeds on at least 87 distinct plant species from over 40 different plant families. Young leaves, shoots, stalks, bolls, buds, and fruits are preferred by *S. littoralis* larvae [32]. Because of its polyphagous nature, *S. littoralis* has harmed various commercially important crops, including cotton, tomato, maize, and other vegetables. The majority of the damage is due to significant larval invasion [33]. Cotton has been one of *S. littoralis*' primary targets. Cotton leaves, flower buds, fruiting tips, and bolls are all eaten, rendering the plant unfit for future use. Egypt is the country with the most cotton damage. Numerous attempts have been undertaken to remove *S. littoralis* due to its catastrophic effect on crops. There are two types of protective methods: biological and chemical. The use of parasites or predators are examples of biological approaches. Chemical insecticides, such as organophosphorus, have also been utilized, despite the fact that these chemicals are harmful to human health. To overcome this difficulty, scientists have turned their attention to AgNPs, a revolutionary and environmentally friendly pesticide that could serve as a potential interface between nanotechnology and pesticides. When compared to traditional physical and chemical synthesis methods, the green method has various advantages, including the absence of highly toxic substances and a high energy need, as well as the fact that it is inexpensive, readily available, and simple to create. These nanoparticles are effective against a variety of agricultural pests. It has been shown that AgNPs exposure causes morphologic abnormalities and DNA damage, as well as negative effects on enzyme activity. We face significant obstacles in employing AgNPs as a pesticide in this work [34]. AgNPs' strong adhesion, small size, and total coverage of the insect body parts with a large surface area resulted in decreased motor functioning and insect mortality. The insect's cuticular lipids triggered physisorption, which resulted in substantial body damage and death. AgNPs could be employed as an alternate antibiotic for extending bull sperm without having a substantial cytotoxic effect on sperm during colt production. [35].

Silver nanoparticles (AgNPs) are ideal for drug delivery systems because they have a large surface area, good biocompatibility, facile surface modification, and appropriate cell penetration[36]. Spermine may efficiently enhance the antibacterial activity of AgNPs, implying that it could be used as an adjuvant to AgNPs to treat a variety of infectious disorders while also minimizing the need of silver antibacterial treatments [37]. Previously, researchers used $NaBH_4$ to investigate the catalytic efficiency of silver nanoparticles in the reduction of 2,4-Dinitrophenol to 2,4-Diaminophenol. We report a simple and ecologically friendly method for the synthesis and characterization of AgNPs. In addition to, we investiged their antibacterial, anticancer, and pesticide properties. Furthermore, the catalytic application of the prepared AgNPs for the $NaBH_4$ reduction of 2,4-Dinitrophenol to 2,4-Di- aminophenol was investigated.

2 Experimental Methods

2.1 Material

Silver nitrate ($AgNO_3$), 2,4-Dinitrophenol and $NaBH_4$ was purchased from Sigma–Aldrich with purity ≥ 99.8%, based on trace metal analysis.

2.1.1 Plant Collection

M. oleifera leaves were collected from Sohag, Egypt (Shandaweel Research center). Leaf extracts were used in the present study because it is proven to reduce silver ions (Scheme 1).

2.1.2 *Moringa oleifera* Extract Preparation

M. oleifera leaves were obtained fresh and washed in double-distilled water. The leaves were broken into small pieces, and 20 g were weighed and added to 200 mL distilled water, which was then boiled to 60 °C, filtered through filter paper, and kept at 4 °C as *M. oleifera* leaf extract (MO).

Scheme 1 Image of *Moringa oleifera* leaves

2.2 Preparation of Aqueous Solution of Ag^+ Ions

We prepared a stock solution of Ag^+ ions by weighing out 0.085 g of $AgNO_3$ and dissolved it in a 0.1-l flask to a final concentration of 5 mM.

2.3 Synthesis of Silver Nanoparticles Loaded by Moringa MOAgNPs

With continual stirring, 10 mL of MO was added to 90 mL of 2 mM $AgNO_3$ in this experiment. Within 10 min, the colour of the mixture had changed from pale yellow to dark brown, indicating the formation of MOAgNPs, which were subsequently centrifuged and collected.

2.4 Structural Investigation of MOAgNPs via Different Techniques

To determine AgNPs, a UV–vis spectrophotometer (Shimadzu UV-PC, Mumbai, India) with a resolution of 1 nm between 200 and 800 nm was utilised. The functional groups of the phytochemical substances in the MO were identified using an FT-IR spectroscope (FTIR-2000, PerkinElmer, Inc.), which capped the AgNPs (MOAgNPs) in the region of 200–4000 cm^{-1}. The average distribution of silver nanoparticle size was analysed using a DLS (Zeta sizer, Malvern Instruments Ltd., U.K.). To produce the AgNPs, the dark-brown liquid was centrifuged for 35 min (EBA 20 zentrifugen 78532, Tuttlingen, Germany). The XRD pattern of the examined AgNPs was determined using Cu-K1 radiations (1.54060) on a PerkinElmer D8 advance (Bruker, Germany). The anode was operated at 30 kV and 15 mA, and the two angles were measured between 5 and 80 degrees. The absorbance at 570 nm was measured using a microplate absorbance reader (2300 EnSpire Multilabel Plate Reader, Perkin Elmer, USA). (TEM, Philips model CM 200, Tokyo, Japan) was used to evaluate the morphology and particle size of the AgNPs.

2.5 Biological Application Protocols

2.5.1 The Pesticide Activity of the Prepared MOAgNPs

The studied larvae were collected from an S. littoralis culture at the Shandaweel Agricultural Research Station's laboratory. For numerous generations, larvae were grown on fresh castor bean leaves without the use of insecticides. The culture was grown in a laboratory setting. (27 ± 2 °C and 55–65% relative humidity; RH).

Laboratory experiments were conducted to determine the toxic activity of the extracts against the fourth instar of *S. littoralis* larvae reared at 27 ± 2 °C and 55–65% RH, and different concentrations of the extract were prepared. The percent of MO: $AgNO_3$ were 5:95 (A), 10:90 (B), 35:65 (C), 65:35 (D), 95: 5(E), and 100:0 (F). Fresh castor leaves were dipped in the various extracts for 20 s each. They were then dried in the shade. 350 larvae were separated into five duplicates, each containing ten larvae, and stored in plastic containers. The larvae were put onto new castor leaves after 24 h of eating and grown up to adulthood. Each trough was filled with 2 to 3 inches of thick sterilized moist sand for pupation in the pre-pupal stage. For adult emergence, the pupae were housed separately in glass troughs. Larval mortality was examined on a daily basis till pupation. Mortality percentage and the corrected mortality percentage were determined using the following formulas:

$$\% \text{ Mortality} = (\text{No. of dead larvae}/\text{Total No. of larvae}) \times 100 \quad (1)$$

$$\text{Corrected \% mortality} = ((X-Y)/(100-Y)) \times 100 \quad (2)$$

where X is the % mortality in treatment, and Y is the % mortality in control. Also, pupal mortality was calculated according to the previous formula. The percentages of malformed pupae, malformed adults, and adult emergence were calculated.

$$\% \text{ Malformed pupae} = ((\text{No. of malformed pupae})/(\text{Total No. of pupae})) \times 100 \quad (3)$$

$$\% \text{ Malformed adults} = ((\text{No. of malformed adults})/(\text{Total No. of adults})) \times 100 \quad (4)$$

$$\% \text{ Emergence} = ((\text{No. of emerged adults})/(\text{Total No. of adults})) \times 100 \quad (5)$$

2.5.2 The Cytotoxic Effect of MOAgNPs

The cytotoxic effect of MOAgNPs against colon carcinoma cells (HCT-116 cell line), hepatic cellular carcinoma cells (HepG-2) and breast carcinoma cells (MCF-7) were assessed. The absorbance of each sample was determined using a microplate absorbance reader (2300 EnSpire Multilabel Plate Reader—Perkin Elmer, USA) at 570 nm using the sulphorhodamine- B (SRB) method. IC_{50} values (half maximal inhibitory concentration) was calculated from the following equation [38–41]:

$$\mathrm{IC50} = \frac{control\ OD - compound\ OD}{control\ OD} \times 100 \quad (6)$$

2.5.3 Antimicrobial Activity of MOAgNPs

The antimicrobial activity of AgNPs was evaluated using an agar disc diffusion test against human pathogenic bacteria and fungi with different concentrations of AgNPs (10 and 20 µg/mL) AgNPs. Vancomycin was used as a standard antibacterial agent. After the incubation period, clear zones around each disc were viewed for confirmation of microbial activity and were measured. The standard deviation reported for each type of nanoparticle and with each microbial strain was based on three replicates. The minimum inhibitory concentration (MIC) of the prepared AgNPs was determined using the serial dilution method. A sterile multi-well ELISA plate (300 µL) was used, each well containing 180 µl of nutrient broth. The plates were kept in an incubator at 37 °C until the colonies appeared. All the experiments were carried out in triplicate. Furthermore, the activities of the prepared AgNPs were evidenced by calculating the activity index according to the relation [42–45]:

$$\mathrm{Activity\ index} = \frac{\mathrm{inhibition\ zone\ OF\ AgNPs\ (mm)}}{\mathrm{inhibition\ zone\ OF\ standard\ drug\ (mm)}} \times 100 \quad (7)$$

2.5.4 The Catalytic Reduction of 2, 4-Dinitrophenol

A quartz spectrophotometer cuvette was used to catalyze the reduction of 2, 4-Dinitrophenol and the process was monitored using a UV/vis absorption spectrophotometer. In the presence of $NaBH_4$ and in the absence of AgNPs catalyst, the reductions of 2, 4-Dinitrophenol were studied. The cuvette was filled with 20 µl of 0.01 M 2, 4-Dinitrophenol ethanol solution and 1800 µl of pure water. To initiate the reaction, 150 µl of 0.1 M $NaBH_4$ was added to the mixture. Second, in order to assess AgNPs' catalytic activity, the reduction process was examined in the presence of AgNPs. 20 µl of 0.01 M 2, 4-Dinitrophenol was mixed with 1700 µl of water, then 80 µl of 1 mM AgNPs colloids and 150 µl of 0.1 M $NaBH_4$ solution was added. The absorption spectrum was recorded at room temperature (25 °C).

3 Results and Discussion

3.1 Characterization of AgNPs

3.1.1 UV/Visible

A UV/Visible absorption spectrometer was used to characterize MO and MOAgNPs at first (Fig. 1). Because MO contains reducing and capping agents that assist to reduce Ag^+ ions, creating MOAgNPs, adding the pale yellow MO to the colorless $AgNO_3$ solution resulted in a dark-brown material [46]. MOAgNPs' surface plasmon resonance (SPR) caused the colour to alter. Because of the chemical compound in the extract, the absorption spectra of MO has an observable peak. The amino acids reduced and stabilized MOAgNPs, as seen by a peak at 385 nm, which is characteristic for absorption of flavonoids and phenols, and a peak at 289 nm in the spectra [47–49]. The synthesized MOAgNPs showed an SPR peak at 440 nm, which suggests AgNP formation [50].

3.1.2 FT-IR Analysis

FT-IR analysis of MO and MOAgNPs was carried out (Fig. 2). The functional groups of MO were indicated using the FT-IR spectra. The region of 1000–1200 cm^{-1} has a peak of cellulose [51]. A peak at 3308 cm^{-1} was due to the O–H and NH_2 groups, which was shifted to 3014 cm^{-1} in MOAgNPs spectrum as the binding of the amino and hydroxyl groups with Ag^+ ions [52]. Peak at 1075 cm^{-1} represents the C–N stretching, while peak at 1120 cm^{-1} represents the C–N group's binding to Ag^+ ions [53]. A peak at 1642 cm^{-1}, corresponding to the amide bond of proteins formed by carbonyl stretching, was shifted to 1620 cm^{-1}, due to the interaction of carbonyl groups with Ag^+ ions [54]. The peak

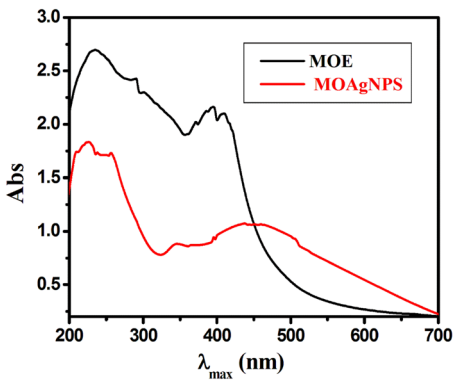

Fig. 1 Molecular absorption spectra of MO and MOAgNPs

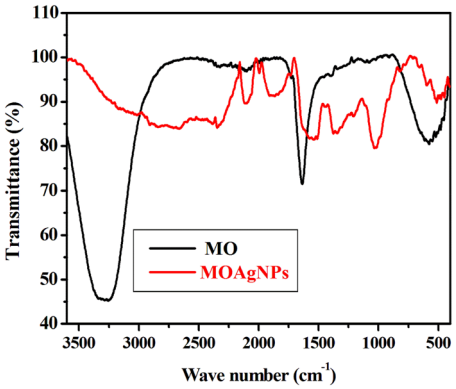

Fig. 2 FT-IR spectra of MO and Ag-loaded *Moringa oleifera* extract (MOAgNPs)

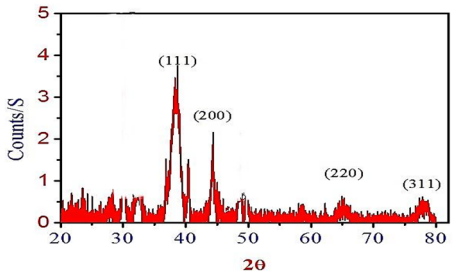

Fig. 3 XRD pattern of synthesized MOAgNPs

at 1398 cm^{-1} was displaced to 1377 cm^{-1}, indicating the bonding between the –OH/COO^- groups and Ag^+ ions, and was attributed to the stretching of –C–O and –C–O–C [4, 5, 55–57]. The MO phytochemical compounds that act as capping and reducing agents of Ag^+ to Ag^0 showed multiple peaks in the synthesised AgNPs.

3.1.3 XRD Analysis of the Silver Nanoparticles

The crystal structure of AgNPs was determined using XRD technique. The peak values in Fig. 3 reveal that the XRD pattern of MO -AgNPs has an FCC system and crystalline lattice at 2θ of 38.12°, 44.3°, 64.45° and 77.42° corresponding to (111), (200), (220), and (311) reflections of AgNPs, and these planes correspond to the standard JCPDS, file number 04-0783 [58].

3.1.4 Dynamic Light Scattering (DLS)

The average diameter of AgNPs was determined using DLS. Figure 4 depicts the average particle size distribution of AgNPs with a mean particle size of 100 nm.

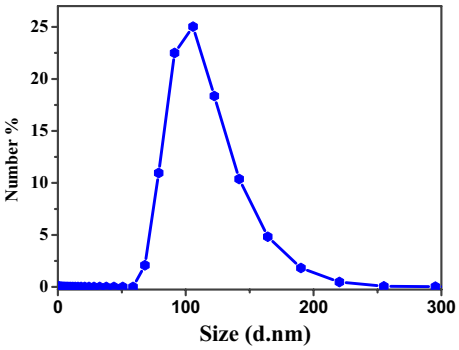

Fig. 4 The particles size distribution of AgNPs

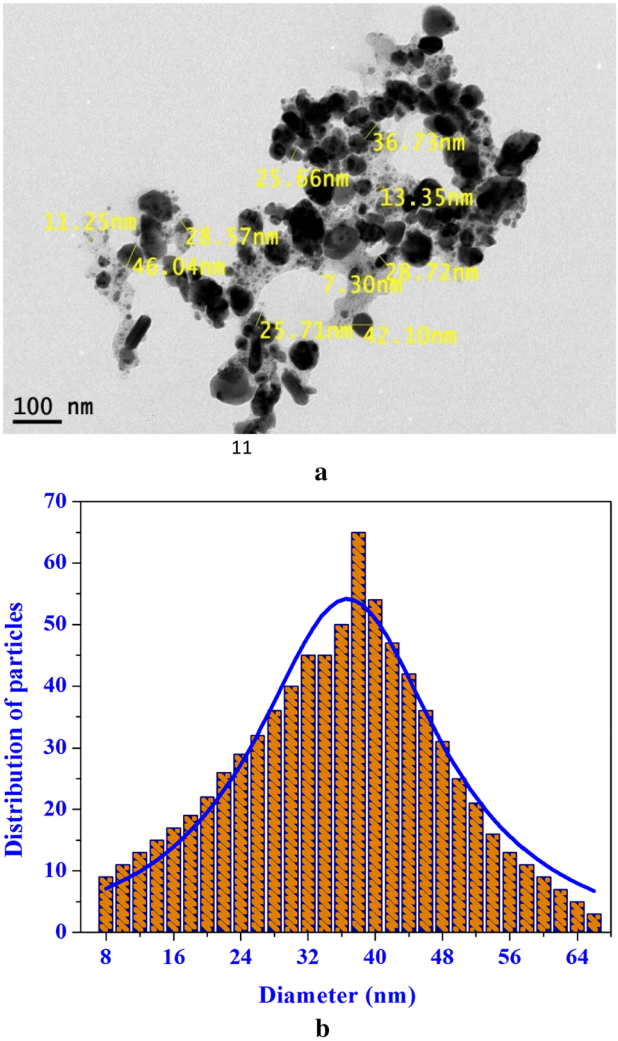

Fig. 5 **a** Size and surface morphology of synthesized MOAgNPs by TEM. **b** Particle size distribution of the prepared AgNPs

Table 1 The effects of MO and the synthesized MOAgNPs on *S. littoralis* larval mortality

Treatments	Larval mortality % after			
	1 day	2 days	3 days	Mean
A	10.00	18.00	18.00	15.33
B	26.00	36.00	42.00	34.67
C	28.00	30.00	30.00	29.33
D	20.00	24.00	24.00 B	22.67
E	28.00	30.00	30.00	29.33
F	10.00	14.00	16.00	13.33

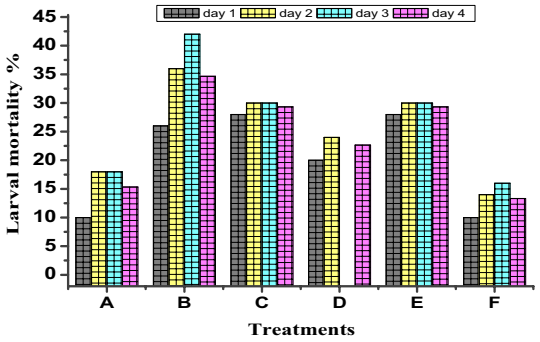

Fig. 6 The effects of MO and the synthesized MOAgNPs on *S. littoralis* larval mortality

3.1.5 TEM Analysis

The transmittion electron microscopy (TEM) technique was used to examine the shape and particle size of the produced MOAgNPs. The majority of the MOAgNPs were spherical, as seen in the TEM image (Fig. 5a). TEM was used to examine the size and morphology of AgNPs. TEM images of AgNPs were spherical in shape. The nanoparticles' average diameter ranges from 5 to 50 nm, with an average particle size of 38.7 nm. Figure 5b. The size distribution of AgNPs has been determined to have a mean diameter of 100 nm at DLS. Due to the hydrodynamic size of nanomaterials, this size is bigger than the TEM data.

3.2 Biological Effect of MO-AgNPs

3.2.1 *Pesticidal* Effect *of MO-AgNPs*

3.2.1.1 Larval Mortality The larval mortality after 1, 2, and 3 days from treatment, as well as the mean effect, are shown in Table 1. It is obvious that the various treatments differed greatly. In all treatments, the data revealed that larval mortality increased as time increased. After 1 day of treatment, two significant groups were observed. The higher values were in groups B (26.00%), C (28.00%), D (20.00%), and E (28.00%); however, the lowest one was in groups A (10.00%) and F (10.00%). After 2 days, the highest mortality was recorded in group B (36.00%), followed insignificantly by groups C (30.00%) and E (30.00%). However, the lowest larval mortality was recorded in group F (14.00%) with the insignificant difference from group A (18.00%). After 3 days, the highest larval mortality was obtained from group B (42.00%), whereas the lowest mortality was observed in group F (16.00%), followed insignificantly by groups A (18.00%) and D (24.00%). According to the mean effect, the highest larval mortality was recorded in group B (34.67%), followed insignificantly by groups C (29.33%) and E (29.33%). On another note, group F recorded the lowest effect (13.33%) with an insignificant difference from group A (15.33%) (Fig. 6).

3.2.1.2 Pupae and Adults The biological effects of MO and the synthesized MOAgNPs on the health of pupal and adult *S. littoralis* are shown in Table 2. The variations between treatments were significant, according to pupal mortality. When compared to the control group, all treatments were effective. The highest pupal mortality was recorded in group A (45.28%), insignificantly followed by groups F (40.93%) and B (36.00%). However, the lowest pupal mortality was observed in group D (23.88%) with an insignificant difference from groups B (36.00%), C (31.00%), and E (27.33%). The tested treatments significantly varied in terms of malformed pupae percentages. All treatments reduced the normal formation of pupae, compared with the control, except for group A. The highest malformed pupae percentage was obtained from group C (28.57%), insignificantly followed by groups B (24.00%) and F (21.67%), whereas the lowest malformed pupae percentage was obtained from group A (2.50%), significantly followed by group D (13.33%). Also, the tested substances significantly varied in adult emergence percentage. It is evident that all MO reduced adult emergence, compared with control. The highest effect was recorded in group A (54.72%), followed insignificantly by groups F (59.07%) and B (64.00%). On another note, groups D and E recorded the lower effect with 76.12% and 72.67%, respectively, with an insignificant difference between them on one side, and with groups C (69.00%) and B on the other side. The malformed adult percentage recorded in the seven treatments significantly varied. Data revealed that group F gave the highest malformed adult percentage with 28.67%. Compared with the control, the rest of the treatments had no effect on the pupal stage. All the tested treatments produced lower numbers of adults, compared with the control. The highest effect was recorded in group F (37.78%), followed insignificantly by groups C (45.71%), B (48.00%), and A (51.15%).

On another note, the lowest effect was obtained from group D (65.83%), insignificantly followed by groups E (57.62%) and A (Figs. 7, 8). Insects are poisoned by AgNPs

Table 2 The effect of MO and the synthesized MOAgNPs on pupation of *S. littoralis*

Treatment	Pupal mortality	Malformed pupae%	Adult Emergence %	Malformed Adult %	Final adults %[a]
A	45.28	2.50	54.72	6.67	51.15
B	36.00	24.00	64.00	0.00	48.00
C	31.00	28.57	69.00	6.67	45.71
D	23.88	13.33	76.12	0.00	65.83
E	27.33	16.90	72.67	5.00	57.62
F	40.93	21.67	59.07	28.67	37.78
Control	0.00	0.00	100.00	2.00	98.00

[a]The percentage of total normal adults obtained from undead larvae

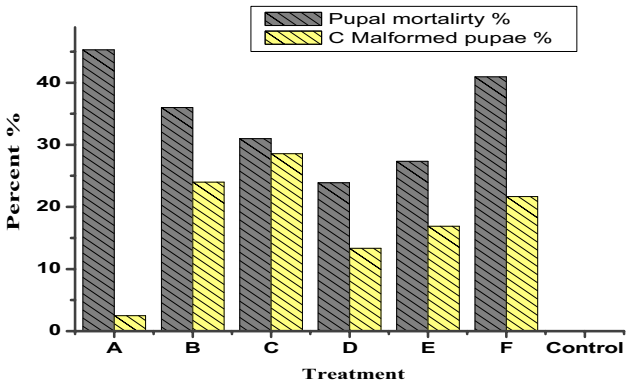

Fig. 7 The effects of MO and the synthesized MOAgNPs on pupal malformation and mortality of *S. littoralis*

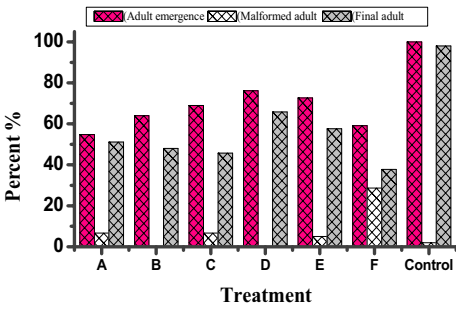

Fig. 8 The effects of MO and the synthesized MOAgNPs on adult emergence and malformation of *S. littoralis*

due to their cytotoxicity and genotoxicity. Nanoparticles cause toxicity by inducing oxidative stress and penetrating the exoskeleton, according to the most widely recognized explanation. The nanoscale substance then binds to sulphur from proteins or phosphorus from DNA in the intracellular space, causing organelles and enzymes to denaturation quickly. As nanoparticles pass past cellular barriers and generate toxic ions that disrupt the cell's machinery, resulting in cell death. Acute and chronic toxicity were observed with AgNPs (pupation, emergence, and reproduction failure) [32–34]. Insects subjected to AgNPs also lost melanin cuticular pigments, resulting in a lighter body. In addition, after eating AgNPs-contaminated diet, their fertility and vertical mobility abilities were greatly decreased. The nanomaterials' high adhesion to the insect body parts resulted in reduced motor functioning and insect death. Physisorption by the insect cuticular lipids resulted in significant injury and mortality. AgNPs cause a buildup of reactive oxygen species (ROS) in insect tissues, resulting in DNA damage, and autophagy [29] as shown in Table 3 and Fig. 9. The antibacterial action was attributed to the biosynthesized MOAgNPs, as there was no zone of inhibition in the negative control. AgNPs have antibacterial activity close to vancomycin when compared to standard antimicrobials [31]. Also, minimum inhibition concentration (MIC) was determined as shown in Table 4. Gram-positive bacteria (*Staphylococcus aureus* and *Bacillus subtilis*) have higher antibacterial activity than Gram-negative bacteria (Serratia marcescens and *Escherichia coli*). MOAgNPs have antibacterial activity close to Vancomycin when compared to standard antibacterial agents. MOAgNPs' antibacterial action could be attributed to their silver ions. When bacteria interact with Ag^+, their membrane permeability increases, causing significant changes in bacterial membrane structure. Because of electrostatic attraction, Ag^+ from MOAgNPs binds to the cell wall and then ruptures it, causing protein denaturation and cell lysis. Furthermore, DNA molecules have become more compact, and the ability to replicate has been lost [59, 60]. The Ag^+ ions interact with proteins via the–SH groups, thereby inactivating them [61]. MOAgNPs can adhere to the microorganisms' cell wall due to their smaller size than the bacteria, causing cell death. In addition, results were compared to zones of inhibition of AgNPs produced from various extracts [62–66].

Table 3 Results of the antimicrobial activity evaluation of the prepared MOAgNPs and Vancomycin against different strains of bacteria in comparison with AgNPs synthesized from different extracts

Compounds	Inhibition zone (mm) ± SD							
	Escherichia coli (− ve)		*Serratia Marcescens* (− ve)		*Bacillus subtilis* (+ ve)		*S. aureus (+ ve)*	
Conc. (µg/ml)	10	20	10	20	10	20	10	20
MOAgNPs Current study	9 ± 0.55	22 ± 0.40	14 ± 0.25	24 ± 0.95	17 ± 0.88	34 ± 0.79	17 ± 0.12	33 ± 0.17
Vancomycin	13 ± 0.05	25 ± 0.16	17 ± 0.17	28 ± 0.20	23 ± 0.14	40 ± 0.22	18 ± 0.16	35 ± 0.26
Distilled water	0.6 ± 0.44		0.85 ± 0. 12		0.8 ± 0.12		0.7 ± 0.15	
AgNPs of O. tenuiflorum [62]	20	30	–		–		12	25
AgNPs of S. cumini [53]	20	26	–		–		14	26
AgNPs of S.alternifolium [63]	13.4	–	–		12.1		9.2	–
AgNPs of *Leucas aspera* [64]	26.3				23			
AgNPs of *Ocimum gratissimum* [65]	20				16		13	
AgNPs of *Allium giganteum*[66]	14				9.5		12	

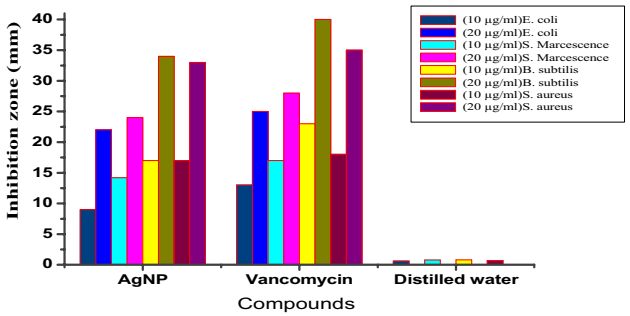

Fig. 9 Antibacterial activity evaluation of the investigated MOAgNPs compared to Vancomycin against different strains of bacteria

Table 4 The results of minimum inhibition concentration (MIC) of MOAgNPs against different strains bacteria

Compound	Minimum inhibition concentration (MIC) (µg/ml)			
	*E.*coli (− ve)	*S.*marcescence (− ve)	*S. aureus* (+ ve)	*B.*subtilis (+ ve)
AgNPs	5.70	4.10	3.15	2.75

3.2.2 Antibacterial Activity of the Synthesized Silver Nanoparticles (MOAgNPs) Against Different Strains of Bacteria

The antibacterial efficacy of biosynthesized MOAgNPs against specific pathogens was assessed using zones of inhibition of the positive control, vancomycin, and the negative control, distilled water, at various doses. (10 and 20 µg/ml) are shown in Table 3 and Fig. 9. The antibacterial action was attributed to the biosynthesized MOAgNPs, as there was no zone of inhibition in the negative control. AgNPs have antibacterial activity close to vancomycin when compared to standard antimicrobials [31]. Also, (MIC) was determined as shown in Table 4. Gram positive bacteria (Staphylococcus aureus and Bacillus subtilis) have higher antibacterial activity than Gram negative bacteria (Serratia marcescens and Escherichia coli). MOAgNPs' antibacterial action could be attributed to their silver ions. When bacteria interact with Ag^+, their membrane permeability increases, causing significant changes in bacterial membrane structure. Because of the electrostatic attraction, Ag^+ from MOAgNPs binds to the cell wall and then ruptures it, causing protein denaturation and cell lysis. Furthermore, DNA molecules have become more compact, and the ability to replicate has been lost. [59, 60]. The Ag^+ ions interact with proteins via the–SH groups, thereby inactivating them [61]. MOAgNPs can adhere to the microorganisms' cell wall due to their smaller size than the bacteria, causing cell death. In addition, results of antimicrobial efficacy of the investigated MOAgNPs were compared to zones of inhibition of AgNPs produced from various extracts and found to be more efficient [62–66].

3.2.3 Cytotoxic Potency of AgNPs Against Human Carcinoma Cells

Table 5 and Fig. 10 show the cytotoxic effect of AgNPs on (HCT-116), (HepG-2) and (MCF-7). The percentage changes were calculated as compared to untreated control cells (DMSO treated). (IC_{50}) values of synthesized AgNPs against (HCT-116 cell line), (HepG-2 cell line), and (MCF-7 cell line) were 6.51, 4.75, and 5.54 µg/ml, respectively, when

Table 5 (IC_{50}) values of MOAgNPs against (HCT-116), (HepG-2) and (MCF-7) cancer cell lines in comparison with AgNPs synthesized form different extracts

Compounds	IC_{50} (µg/ml)		
	MCF-7	HCT-116	HepG-2
MOAgNPs Current study	5.54 ± 0.15	6.51 ± 0.66	4.75 ± 0.34
DMSO	0.00	0.00	0.00
Doxorubicin	4.45 ± 0.15	5.25 ± 0.12	4.25 ± 0.13
AgNPs of Cyanobacterium *Oscillatoria limnetica* [67]	6.15 ± 0.13	5.37 ± 0.23	–
AgNPs of *Ocimum Kilimandscharicum* [68]	–	–	4.9
aAgNPs of *Erythrina indic* [69]		23.89	
AgNPs of *Melia dubia* [70]		31.2	
AgNPs of *Achillea biebersteinii* [71]		20	

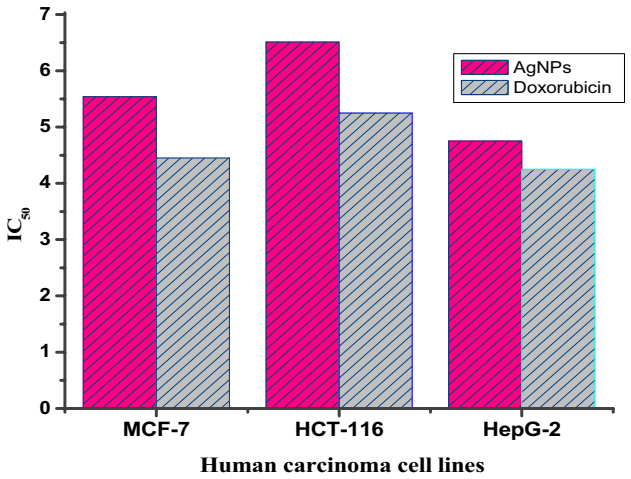

Fig. 10 IC_{50} values of MOAgNPs against (HCT-116), (HepG-2) and (MCF-7) cell lines

compared to the (IC_{50}) values of Doxorubicin, which were 5.25, 4.25, and 4.45 µg/ml, respectively. AgNPs have a cytotoxic effect similar to Doxorubicin, with the HepG-2 and MCF-7 cell lines being more responsive to AgNPs treatment than the HCT 116 colon cancer cell lines. AgNPs inhibited cell growth in HepG-2 cells with an IC_{50} value of 4.75 µg /ml, whereas the HCT-116 cell line had an IC_{50} value of 6.51 µg/ml. AgNPs have a cytotoxic effect similar to Doxorubicin, with the HepG-2 and (MCF-7) being more responsive to AgNPs treatment than (HCT 116). AgNPs inhibited cell growth in HepG-2 cells with an IC_{50} value of 35 µg/ml, whereas the HCT-116 cell line had an IC_{50} value of 6.51 µg/ml [61]. The (IC_{50}) values of the synthesized AgNPs form different extracts [67–71] against MCF-7, HCT-116 and HepG-2 are shown in Table 5 compared to MOAgNPs and standard drug Doxorubicin. Thus, the simple and green biogenic synthesis of silver nanoparticles (AgNPs) provides not only AgNPs with extraordinary characteristics, but also cost-effective, readily available, and surprisingly biologically active nanoparticles. [72–75]

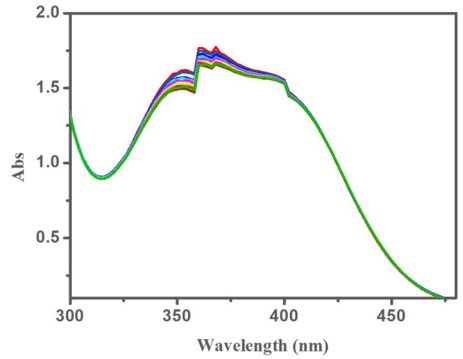

Fig. 11 Absorption spectra for 2,4- Di-nitrophenol reduction in the absence of MOAgNPs

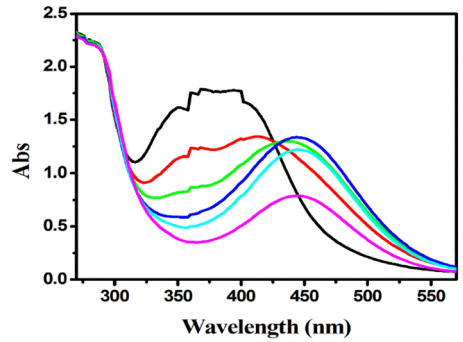

Fig. 12 Absorption spectra of the catalytic reduction of 2, 4-Dinitrophenol catalyzes by MOAgNPs at first 10 min

3.3 MOAgNPs for Catalytic Reduction of 2, 4-Dinitrophenol to 2, 4-Di-Aminophenol.

Nanomaterials due to their facenating properities they are used as catalysts for some chemical reaction [76–78]. MOAgNPs can be used as a catalyst for a chemical reactions [79, 80]. 2, 4-Di-nitrophenol showed its strongest absorption peak at 368 nm as shown in Fig. 11. Atoms in the 2,4-Dinitrophenol structure (Oxygen and nitrogen) have

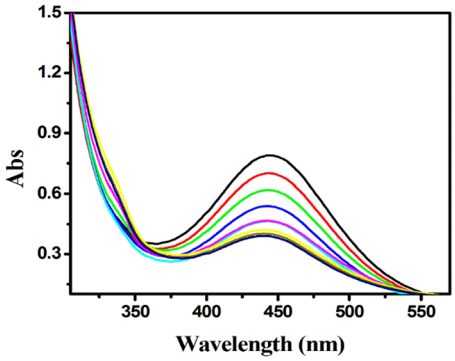

Fig. 13 Absorption spectra of the catalytic reduction of 2, 4-Dinitrophenol catalyzes by MOAgNPs at next 20 min

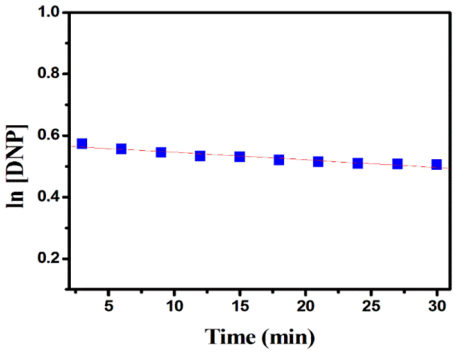

Fig. 14 ln [2, 4- Di-nitrophenol] versus time plots without catalyst for 2, 4- Di-nitrophenol reduction

electrons gave rise to the electronic transition n-π*. This peak remained stable for an hour, showing that the reaction is unable without catalysis.

Absorption spectrum of 2, 4-Dinitrophenol by adding Sodium borohydride and MOAgNPs as catalyst was determined (Figs. 12, 13). After 10 min, the peak at 368 nm decreased due to decreased 2, 4-Dinitrophenol concentration, and new peaks at 287 and 443 nm appeared, indicating the formation of 2, 4-Dinitrophenolate ion and 2, 4-Diaminophenol. After 20 min, the peaks at 287 and 443 nm decreased, a new small distinctive band around 314 nm developed, and the spectra became steady, suggesting that the 2,4-Dinitrophenolate intermediate changed into 2,4-Diaminophenol (DAP). The solution's coloring changed from yellow to pale orange. [77, 81, 82]

The rate constant was estimated from the reduction in intensity of the absorption peak at 368 nm over time in order to evaluate the catalytic activity of silver nanoparticles. The rate constant can be determined from the linear relationship between ln A and time because the concentration of $NaBH_4$ is constant. From curves, the rate constants (k, min^{-1}) were found to be 2×10^{-3} min^{-1} and 24×10^{-3} min^{-1} for the reaction without any silver nanoparticles and (MOAgNPs)

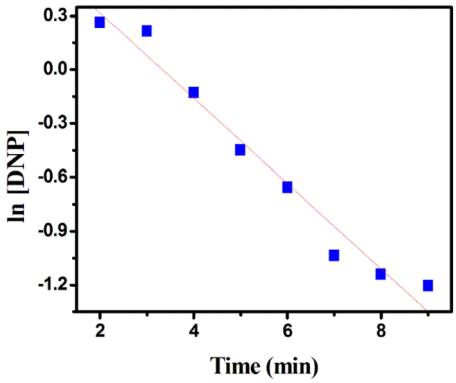

Fig. 15 ln [2, 4- Di-nitrophenol] versus time plots using MOAgNPs as catalysts for 2, 4- Di-nitrophenol reduction

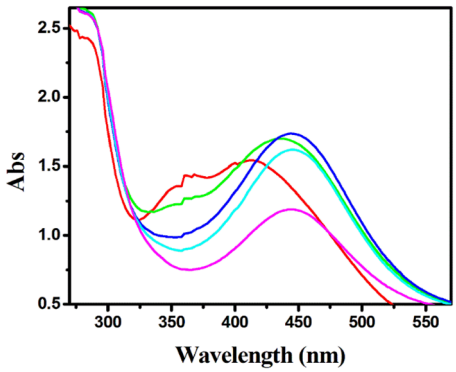

Fig. 16 Absorption spectra of 2, 4-Dinitrophenol catalytic reduction catalyzes by MOAgNPs in the second cycle

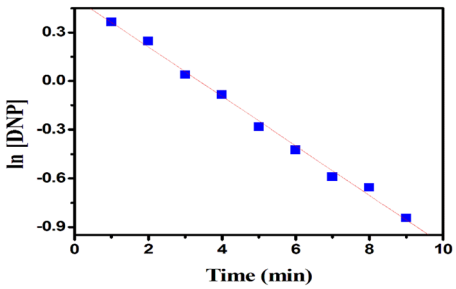

Fig. 17 ln [2, 4- Dinitrophenol] with time (min.) using MOAgNPs as catalyst for 2,4- Di-nitrophenol reduction in the second cycle

respectively Figs. 14 and 15. When these 2, 4-Di-nitrophenol reduction rate constants are compared, it is clear that silver nanoparticles accelerated the process and had good catalytic activity.

To test the recycling ability of the catalyst, AgNps were separated from reaction mixture by centrifugation and were re-used for catalytic reduction of 2, 4-Dinitrophenol. Activity of MOAgNps catalyst for catalytic reduction

of 2, 4-Dinitrophenol is studying by UV/vis spectra of the catalytic reduction of 2, 4-Dinitrophenol as shown in Fig. 16. Rate constant of the reactions was calculated from the decrease in intensity of the absorption peak over time Fig. 17. The following given relation shows the activity of the catalyst:

$$\text{Percenatge activity} = \frac{\text{k 2}}{\text{k 1}} \times 100$$

= where k 1, is the rate constants in first cycle, K2 is the rate constants in the second cycle. The rate constant k 1 was found to be 24.0×10^{-3} min^{-1} for the reaction with silver nanoparticles, (MOAgNPs) in first cycle, k 2 was found to be 15.0×10^{-3} min^{-1} for the reaction with silver nanoparticles, (MOAgNPs) in the second cycle. The percentage activity of MOAgNPs catalyst was found to be 62.5%.

The oxide layer formed on the surface of AgNPs upon air exposure or small leaching of AgNPs during catalysis process explain the decrease in activity of AgNPs as catalysts [83, 84].

3.3.1 The Temperature-Dependent Reduction Process of 2, 4-Dinitrophenol Catalysed by MOAgNPs and Thermodynamics Study

We examined the temperature-dependent reduction process of 2, 4-Dinitrophenol catalysed by MOAgNPs. The effect of temperature on the k values was examined from 293 to 313 K. The k values for the reduction of 2, 4-Dinitrophenol increased with the increase in temperature as the increase in the diffusion, as shown in Table 6, Figs. 18.

The Arrhenius equation was used to calculate the activation energies (E_a) for the 2, 4-Dinitrophenol reduction process.

$$\ln k = \ln A - E_a/RT \quad (8)$$

The activation parameters and Ea values were calculated using the slope of the plot of ln k vs. 1/T, as illustrated in Fig. 19 and Table 7.

The Ea values for the reduction of nitrophenol catalysed by various metal NPs have been determined. For the reduction of 4-nitrophenol with palladium NPs and a palladium nanocage structure, the Ea values are 30 kJ mol^{-1} and 109 kJ mol^{-1}, respectively [85]. The activation energies Ea for 2, 4-Dinitrophenol catalysed by MOAgNPs are 44.2 kJ mol^{-1}, confirming the L–H mechanism. The Eyring equation was used to calculate the activation enthalpy (H*) and activation entropy (S*) for the reduction of 2,4-Di-nitrophenol.

$$\ln\left(\frac{k}{T}\right) = \ln\left(\frac{kB}{h}\right) + \frac{\Delta S^*}{R} - \frac{\Delta H^*}{RT}$$

$$\Delta G^* = \Delta H^* - T\Delta S^*$$

The thermodynamic parameters were calculated using Fig. 20 and Table 7. The values of k constant for 2, 4-Dinitrophenol were 0.042 min^{-1}, catalyzed by MOAgNPs. Using the reduction of 2, 4-Di-nitrophenol, thermodynamic parameters ΔH^*, ΔS^*, and ΔG^* were 41.7 kJ mol^{-1}, –116.4 J mol^{-1} K^{-1}, and 76.4 kJ mol^{-1}, respectively, for MOAgNPs catalyst. The change in free energy that occurs when one chemical or a group of chemicals is transformed to one or more other chemicals in their standard forms is known as the standard free-energy change. As indicated by these values, the 2, 4- Di-nitrophenol reduction process is definitely endothermic[85]. In addition, the activation

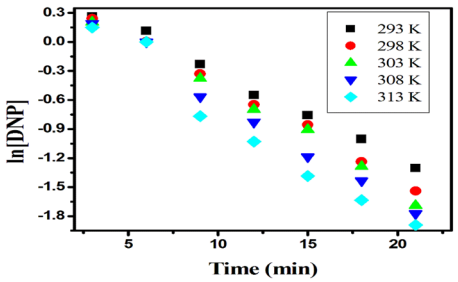

Fig. 18 Temperature effect from 293 to 313 K on the k values of the reduction reaction of 2, 4-Dinitrophenol catalyzed by MOAgNPs

Table 6 Temperature dependent k values for the reduction of 2, 4-Dinitrophenol catalyzed by MOAgNPs

Temperature (K)	k (min^{-1})$\times 10^{-3}$
293	22.6
298	24.0
303	27.2
308	42.2
313	73.4

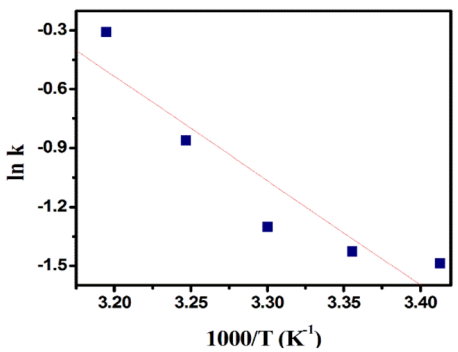

Fig. 19 Plots of ln k vs. 1/T (the Arrhenius) for the reduction reaction of 2, 4-Dinitrophenol

Table 7 Thermodynamic parameters for the reduction reaction of 2, 4-Di-nitrophenol

	Ea (kJ mol^{-1})	ΔH* (kJ mol^{-1})	ΔS* (J mol^{-1} K^{-1})	ΔG* (kJ mol^{-1})
2, 4-Dinitrophenol reduction catalyzed by MOAgNPs	44.2	41.7	-116.4	76.4

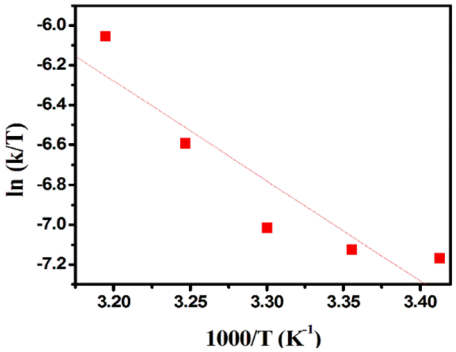

Fig. 20 The Eyring plots of ln k/T versus 1/T for the reduction reaction of 2, 4 di-nitrophenol

parameters H^* and S^* were obtained for use in subsequent investigations. To continue with the reduction reaction, 2, 4-Di-nitrophenol must first overcome the energy barrier by adsorbing on the catalyst surface. As a result, the MOAgNPs have a high catalytic activity.

Mechanism of catalytic reduction reactions follow the Langmuir–Hinshelwood (L–H) mechanism. On the surface of MOAgNPs, the BH_4^- ions were adsorbed to the surface of the MOAgNPs. Also 2, 4-Dinitrophenol adsorbs on the surface of MOAgNPs and is reduced to 2,4-Di-aminophenol by the BH_4^- ions. The catalytic product 2, 4-diaminophenol is separated to free the surface of the MOAgNPs. The catalytic reduction reaction's k values are proportional to the materials' surface area. The MOAgNPs catalyzed reduction of 2, 4-Dinitrophenol occurs according to the L–H mechanism [85, 86]. MOAgNPs synthesized using the green technique have a wide range of applications as catalyst and adsorbent because of high surface area [57].

4 Conclusion

The manufacture of MOAgNPs utilising *M. oleifera* extract was demonstrated in this study. FT-IR and UV/vis spectra revealed the role of phytochemical components in the plant extract, such as amino acids and flavanols for the bio reduction of Ag^+ ions to Ag^0. Dynamic light scattering DLS was used to determine the size and shape of MOAgNPs. The FCC crystal system of MOAgNPs was confirmed by XRD study. The AgNPs' strong adhesion, small size, and total coverage of the insects' body parts with a large surface area resulted in reduced motor functioning and insect mortality. The cytotoxic activity of MOAgNPs (IC_{50}) values against (HCT-116), (HepG-2) and (MCF-7) cell lines was found to be close to the cytotoxic activity (IC_{50}) values of the standard drug Doxorubicin. The synthesized nanoparticles (MOAgNPs) are eco-friendly, inexpensive, and have pesticidal and antibacterial activities against *S. littoralis, Staphylococcus aureus, Bacillus subtitle, Serratia marcescens and Escherichia coli*. The synthesized AgNPs were used for the reduction reaction of 2, 4-Di-nitrophenol by $NaBH_4$ to 2, 4-Diaminophenol. Thermodynamic parameters such as ΔH^*, ΔS^* and ΔG^* for the reduction of 2, 4-Dinitrophenol were 44.2 kJ mol^{-1}, − 116.4 Jmol^{-1} K^{-1} and 76.4 kJ mol^{-1} respectively for MOAgNPs catalyst. From the obtained results it can be concluded that MOAgNPs synthesized using the green technique have a wide range of applications as nanopesticides, anticancer agents, antibacterial agents, and potent catalytic agents in diverse domains.

Declarations

Conflict of interest There are no conflicts to declare.

References

1. D. Mubarak Ali, N. Thajuddin, K. Jeganathan, M. Gunasekaran, Colloid. Surf. B Biointerface **85**, 360 (2011)
2. W.S. Mohamed, M. Alzaid, M.S.M. Abdelbaky, Z. Amghouz, S.G. Granda, A.M. Abu-Dief, Nanomaterials **9**, 1602 (2019)
3. W.S. Mohamed, A.M. Abu-Dief, Ceram. Int. **46**, 16196–16209 (2020)
4. N. Ahmad, S. Sharma, Md.K. Alam, V.N. Singh, S.F. Shamsi, B.R. Mehta, A. Fatma, Colloid Surf. B Biointerfaces **81**, 86 (2010)
5. A.M. Abu-Dief, L.H. Abdel-Rahman, M.A. Abd-El Sayed, M.M. Zikry, A. Nafady, ChemistrySelect **5**(42), 13263–13268 (2020)
6. M.D.M.R. Mollick, B. Bhowmik, D. Maity, D. Mondal, I. Roy, J. Sarkar, D. Rana, K. Acharya, S. Chattopadhyay, D. Chattopadhyay, Microfluid Nanofluid **16**, 541 (2014)
7. A. Singh, D. Jain, M.K. Upadhyay, N. Khandelwal, H.N. Verma, Dig. J. Nano mater. Bio Structs. **5**, 483 (2010)
8. P.S. Retchkiman-Schabes, G. Canizal, R. Becerra-Herrera, C. Zorril-la, H.B. Liu, J.A. Ascencio, Opt. Mater. **29**, 95 (2006)
9. H. Gu, P.L. Ho, E. Tong, L. Wang, B. Xu, Nano Lett. **3**, 1261 (2003)
10. Z. Ahmad, R. Pandey, S. Sharma, G.K. Khuller, Indian J. Chest Dis. Allied Sci. **48**, 171 (2006)
11. K.P. Bankura, D. Maity, M.M.R. Mollick, D. Mondal, B. Bhowmick, M.K. Bain, A. Chakraborty, J. Sarkar, K. Acharya, D. Chattopadhyay, Carbohydr. Polym. **89**, 1159 (2012)

12. M. Farooqui, P.S. Chauhan, P. Krishnamoorthy, J. Shaik, Digest. J. Nanomater. Biostruct. **5**, 43 (2010)
13. K. Cho, J. Park, T. Osaka, S. Park, Electrochim. Acta **51**, 956 (2005)
14. E.K. Elumalai, T.N.V.K.V. Prasad, J. Hemachandran, S.V. Therasa, T. Thirumalai, E. David, J. Pharm. Sci. Res. **2**, 549 (2010)
15. M. Safaepour, A.R. Shahverdi, H.R. Shahverdi, M.R. Khorramizadeh, A.R. Gohari, Avicenna J. Med Biotechnol. **1**, 111 (2009)
16. A.M. Awwad, N.M. Salem, Nano Sci. Nano Technol. **2**, 125 (2012)
17. S.P. Chandran, M. Chaudhary, R. Pasricha, A. Ahmed, M. Sastry, Biotechnol. Prog. **22**, 577 (2006)
18. M.D. Thurber, J.W. Fahey, Ecol. Food Nutr. **48**, 212 (2009)
19. M.I. Grijalva, I.V. Fernandez, J.A. Ponce, E. Artalejo, A. Nieblas, L.E. Gonzalez, A pilot study. FASEB J. **25**, 175 (2011)
20. R.-Y. Yang, S.C.S. Tsou, T.-C. Lee, L.-C. Chang, G. Kuo, P.-Y. Lai, in *Herbs: Challenges in Chemistry and Biology*. ed. by M. Wang (American Chemical Society, Washington DC, 2006), p. 224
21. O. V., Kharissova, 4, **2018**.
22. R. Sood, D.S. Chopra, J. Phymed. **08**, 025 (2017)
23. D. Govindaraj, M. Rajan, Mater. Today Proc. **3**, 2394 (2016)
24. N. Matinise, K. Kaviyarasu, N. Mongwaketsi, S. Khamlich, L. Kotsedi, N. Mayedwa, M. Maaza, Appl. Surf. Sci. **446**, 66 (2018)
25. N. Matinise, X.G. Fuku, K. Kaviyarasu, N. Mayedwa, M. Maaza, Appl. Surf. Sci. **406**, 339 (2017)
26. A.A. Ezhilarasi, J.J. Vijaya, K. Kaviyarasu, M. Maaza, A. Ayeshamariam, L.J. Kennedy, J. Photochem. Photobiol. B **164**, 352 (2016)
27. K. Vasanth, K. Ilango, R. MohanKumar, A. Agrawal, G.P. Dubey, Colloids Surf. B Biointerfaces **117**, 354 (2014)
28. V. Sivaranjani, P. Philominathan, Wound Med. **12**, 1 (2016)
29. L. Katata-Seru, T. Moremedi, O.S. Aremu, I. Bahadur, J. Mol. Liq. **256**, 296 (2018)
30. M. Hussain, A. Nafady, M. Sirajuddin, A. Avcı, E. Pehlivan, J. Nisar, S.T.H. Sherazi, A. Balouch, M.R. Shah, O.A. Almaghrabi, M.A. Ul-Haq, Nanomaterials **9**(11), 1604 (2019)
31. T. Shaikh, A. Nafady, F.N. Talpur, M.H. Agheem, M.R. Shah, S.T.H. Sherazi, Sens. Actuators **211**, 359–369 (2015)
32. H. Salama, N. Dimetry, S. Salem, Zeitschrift für Angewandte Entomologie **67**, 261 (1971)
33. I. Bishara, Bulletin de la Société Entomologique d' Egypte **18**, 223 (1934)
34. G. Benelli, Environ. Sci. Pollut. Res. **25**, 12329 (2018)
35. M.S. Yousef, H.N. Abdelhamid, M. Hidalgo, R. Fathy, L. Gomez-Gascon, J. Dorado, Theriogenology **161**, 219 (2021)
36. L. Qiu, L. Zhao, C. Xing, Y. Zhan, Chin. Chem. Lett. **29**, 301 (2018)
37. C. Liu, H. Shen, S. Wang, X. Cao, H. Xua, Y. Xia, T. Bai, Y. Liu, L. Peng, C. Li, Z. Guo, Z. Li, Chin. Chem. Lett. **2018**, 29 (1824)
38. A.M. Abu-Dief, I.F. Nassar, W.H. Elsayed, Appl. Organomet. Chem. **30**, 917–923 (2016)
39. L.H. Abdel-Rahman, A.M. Abu-Dief, M.R. Shehata, F.M. Atlam, A.A.H. Abdel-Mawgoud, Appl. Organometal. Chem. **33**, e4699 (2019)
40. L.H. Abdel-Rahman, A.M. Abu-Dief, F.M. Atlam, A.H. Abdel-Mawgoud, A.A. Alothman, A.M. Alsalme, A. Nafady, J. Coord. Chem. **73**(23), 3150–3173 (2020)
41. E.T. Aljohani, M.R. Shehata, A.M. Abu-Dief, Appl. Organomet. Chem. **35**(4), e6169 (2021)
42. A.M. Abu-Dief, H.M. El-Sagher, M.R. Shehata, Appl. Organomet. Chem. **33**, e4943 (2019)
43. L.H. Abdel-Rahman, A.M. Abu-Dief, R.M. El-Khatib, S.M. Abdel-Fatah, Int. J. Nano. Chem. **4**, 1 (2018)
44. E.T. Aljohani, M.R. Shehata, F. Alkhatib, S.O. Alzahrani, A.M. Abu-Dief, Appl. Organomet. Chem. **35**, e6154 (2021)
45. A.M. Abu-Dief, R.M. El-khatib, S.M. El Sayed, S. Alzahrani, F. Alkhatib, G. El-Sarrag, M. Ismael, J. Mol. Struct. **1244**, 131017 (2021)
46. M. Darroudi, M.B. Ahmad, A. Abdullah, N. Ibrahim, K. Shameli, Int. J. Mol. Sci. **11**, 3898 (2010)
47. T. Fafal, P.B. Taştan, S. Tüzün, M. Ozyazici, B. Kivcak, S. Afr. J. Bot. **112**, 346 (2017)
48. J. Xie, J.Y. Lee, D.I.C. Wang, Y.P. Ting, ACS Nano **1**, 429 (2007)
49. N. Saifuddin, C.W. Wong, A.A. NurYasumira, *E.J. Chem*., **2009**, 6, 61.
50. B. Rao, R.C. Tang, Adv. Nat. Sci. **8**, 15 (2017)
51. L.H. Abdel-Rahman, A.M. Abu-Dief, M.A. Abd-El Sayed, M.M. Zikry, J. Chem. Mater. Res. **4**, 8 (2016)
52. L.H. Abdel-Rahman, A.M. Abu-Dief, M.A. Abd-El-Sayed, M.M. Zikry, J. Trans. Met. Complex **2018**, 1 (2018)
53. N. Alaguchamy, M. Chandran, J. Pharm. Pharm. Sci. **5**, 11 (2016)
54. T. Biswas, A. Sen, R. Roy, S. Maji, H.S. Maji, J. Pharm. Anal. **4**, 49 (2015)
55. T. Elavazhagan, K.D. Arunachalam, Memecylonedule. Int. J. Nano Med. **6**, 1265 (2011)
56. M.N. Alam, N. Roy, D. Mandal, N.A. Begum, RSC Adv. **3**, 11935 (2013)
57. A.M. Abu-Dief, L.H. Abdel-Rahma, M.A. Abd-El-Sayed, M.M. Zikry, AJACR **9**, 1 (2021)
58. G.C.J. Swarnavalli, S. Dinakaran, N. Raman, R. Jegadeesh, C. Pereira, J. Saudi Chem. Soc. **21**, 172 (2017)
59. M. Buttacavoli, N.N. Albanese, G. Di Cara, R. Alduina, C. Faleri, M. Gallo, G. Pizzolanti, G. Gallo, S. Feo, F. Baldi, P. Cancemi, Oncotarget **9**(11), 9685 (2018)
60. I. Sondi, B. Salopek-Sondi, J. Colloid Interface Sci. **275**, 177 (2004)
61. O. Fellahi, R.K. Sarma, M.R. Das, R. Saikia, L. Marcon, Y. Coffinier, T. Hadjersi, M. Maamache, R. Boukherroub, Nanotechnology **24**, 495 (2013)
62. P. Logeswari, S. Silambarasan, J. Abraham, J. Saudi Chem. Soc. **19**, 311–317 (2015)
63. P. Yugandhar, R. Haribabu, N. Savithramma, 3 Biotech **5**, 1031 (2015)
64. M. Sivaramakrishnan, V. Svanan, G.D. Karaiyagowder, Y. Meganathan, B.S. Devaraj, S. Natesan, R. Kothandan, K. Kandaswamy, Appl. Sci. **1**, 3 (2019)
65. K. Sharma, S. Guleria, V.K. Razdan, J. Plant Biochem. Biotechnol. **29**, 213 (2020)
66. M.E. Taghavizadeh Yazdi, A. Hamidi, M.S. Amiri, R. Kazemi Oskuee, H.A. Hosseini, A. Hashemzadeh, M. Darroudi, Mater. Technol. **34**, 490 (2019)
67. R.A. Hamouda, M.H. Hussein, R.A. Abo-elmagd, S.S. Bawazir, Sci. Rep. **9**, 13071 (2019)
68. S. Selvarani, P.V. Moorthi, P. Saranya, M. Abirami, Nanotechnol. Nanosci. **1**, 100 (2015)
69. P.R. Sre, M. Reka, R. Poovazhagi, M.A. Kumar, K. Murugesan, Spectrochim. Acta Part A Mol. Biomol. Spectrosc. **135**, 1137 (2015)
70. V. Kathiravan, S. Ravi, S. Ashokkumar, Spectrochim. Acta Part A Mol. Biomol. Spectrosc. **130**, 116 (2014)
71. J. Baharara, F. Namvar, T. Ramezani, M. Mousavi, R. Mohamad, Molecules **20**, 2693 (2015)
72. T.M. Ahamad, G.E. Naushad, S.I. Eldesoky, A. Al-Saeedi, J. Nafady, Mol. Liq. **282**, 154–161 (2019)
73. S.S. Hassan, A. Nafady, A.R. Solangi, M.S. Kalhoro, M.I. Abro, S.T.H. Sherazi, Sens. Actuators **208**, 320 (2015)
74. H. Vardhan, G. Verma, S. Ramani, A. Nafady, A.M. Al-Enizi, Y. Pan, Z. Yang, ACS Appl. Mater. Interfaces **11**(3), 3070 (2018)
75. S. Kummara, M.B. Patil, Tiewlasubon uriah, original article synthesis, characterization, biocompatible and anticancer activity of

green and chemically synthesized silver nanoparticles: a comparative study. Biomed. Pharmacother. **84**, 10–21 (2016)
76. S.S. Dash, B.G. Bag, P. Hota, Appl. Nanosci. **5**, 343 (2015)
77. K. Gerelbaatar, A. Tsogoo, R. Dashzeveg, N. Tsedev, E.O. Ganbold, Solid State Phenom. **271**, 76 (2017)
78. S. Kim, W.B. Sang, J.S. Lee, J. Park, Tetrahedron **65**, 1461 (2009)
79. M. Pan, J. Gong, G. Dong, C.B. Mullins, Acc. Chem. Res. **46**, 650 (2013)
80. J. Gong, C.B. Mullins, Acc. Chem. Res. **42**, 1063 (2009)
81. X.-Q. Wu, X.-W. Wu, Q. Huang, J.-S. Shen, H.-W. Zhang, Appl. Surf. Sci. **331**, 210 (2015)
82. K. Karakas, A. Celebioglu, M. Celebi, T. Uyar, M. Zahmakiran, Appl. Catal. B **203**, 549 (2017)
83. K. Naseem, R. Begum, W. Wu, A. Irfan, A.G. Al-Sehemi, Z.H. Farooqi, J. Clean. Prod. **211**, 855–864 (2019)
84. Y. Lu, X. Wan, L. Li, P. Sun, G. Liu, J. Market. Res. **12**, 1832–1843 (2021)
85. S.R. Thawarkar, B. Thombare, B.S. Mundec, N.D. Khupse, RSC Adv. **8**, 38384 (2018)
86. S. Wunder, F. Polzer, Y. Lu, Y. Mei, M.J. Ballauff, J. Phys. Chem. C **114**, 8814 (2010)